Ion charge-resolved branching in decay of inner shell holes in Xe up to 1200 eV

2015 J. Phys. B: At. Mol. Opt. Phys. 48 205001

(http://iopscience.iop.org/0953-4075/48/20/205001)

OPEN ACCESS
IOP Publishing
Journal of Physics B: Atomic, Molecular and Optical Physics
J. Phys. B: At. Mol. Opt. Phys. **48** (2015) 205001 (7pp)
doi:10.1088/0953-4075/48/20/205001

Ion charge-resolved branching in decay of inner shell holes in Xe up to 1200 eV

J H D Eland[1,2], C Slater[1,2], S Zagorodskikh[2,3], R Singh[2], J Andersson[2], A Hult-Roos[2], A Lauer[1], R J Squibb[2] and R Feifel[2]

[1] Department of Chemistry, Physical and Theoretical Chemistry Laboratory, Oxford University, South Parks Road, Oxford OX1 3QZ, UK
[2] Department of Physics, University of Gothenburg, Origovägen 6B, SE-412 96 Gothenburg, Sweden
[3] Department of Physics and Astronomy, Uppsala University, Box 516, SE-751 20 Uppsala, Sweden

Received 23 April 2015, revised 9 July 2015
Accepted for publication 14 July 2015
Published 4 September 2015

Abstract

Using a new multi-electron multi-ion coincidence apparatus and soft x-ray synchrotron radiation we have determined branching ratios to final Xe^{n+} states with $2 < n < 9$ from the $4d^{-1}$, $4p^{-1}$, $4s^{-1}$, $3d^{-1}$ and $3p^{-1}$ Xe^{+} hole states. The coincident electron spectra give information on the Auger cascade pathways. We show that by judicious choice of coincident electrons, almost pure single charge states of the final ions can be selected.

Keywords: inner shell holes, multiple Auger decay, branching ratios, coincidence detection

(Some figures may appear in colour only in the online journal)

Introduction

Although Xe is indeed a well-studied showcase for atomic inner shell ionization as pointed out by Becker *et al* [1], the ultimate fates of states with inner shell holes deeper than the outermost ones, $4d^{-1}$ and $4p^{-1}$ still deserve more detailed study. Here we introduce a new electron–ion coincidence apparatus and use it to measure the final charge distributions directly for all initial pure single hole states up to the $3p^{-1}$ levels. We also show that by selection of the number and energies of coincidently detected electrons we can select formation of almost pure single charge states. This ability, when carried over to molecules, will allow systematic study of the effect of the charge state on the dynamics of dissociation by the so-called Coulomb explosions. The primary objective of this work is to provide a reliable prototype for such studies on molecules containing iodine atoms. In line with this physico-chemical orientation of the work we use the nl_j nomenclature for orbitals instead of the KLMN terminology traditionally used in Auger spectroscopy.

Important previous studies of Xe inner shell processes include the ion yield measurements as a function of photon energy [2–4] and the electron–ion coincidence measurements of Luhmann *et al* [5]. Much detailed insight is given by the electron–electron coincidence measurements of Hikosaka *et al* [6, 7] and the threshold electron–ion coincidence work of Matsui *et al* [8]. High resolution Auger electron spectra have been acquired and analysed in detail after 4d [9, 10] and 3d [11, 12] inner shell hole creation, and interpreted with some identification of the Auger cascades and final ion states, and with theoretical calculation of the rates of the transitions involved. Hartree–Fock calculations of the branching from single hole states have been done by Kochur *et al* [13] including all the significant branching pathways. Most recently a new Monte-Carlo method for efficient calculation of the branching in these processes has been developed by Son and Santra [14] and has been applied to the inner shell ionization of Xe at the high fluences available from an x-ray free-electron laser.

The majority of previous measurements of the branching from inner shell hole states to different charge states of Xe [2–4, 15] have operated on the principle of measuring the yields of Xe^{n+} ions as a function of the soft x-ray energy and observing the steps in yield at each edge. Because of the complexity of the processes that can be induced by x-ray absorption, this method has limitations. In the energy region some eV below a true edge, resonant processes in which an electron is promoted from an inner shell to a normally unoccupied orbital often have large excitation cross-sections and can decay to very different ionized

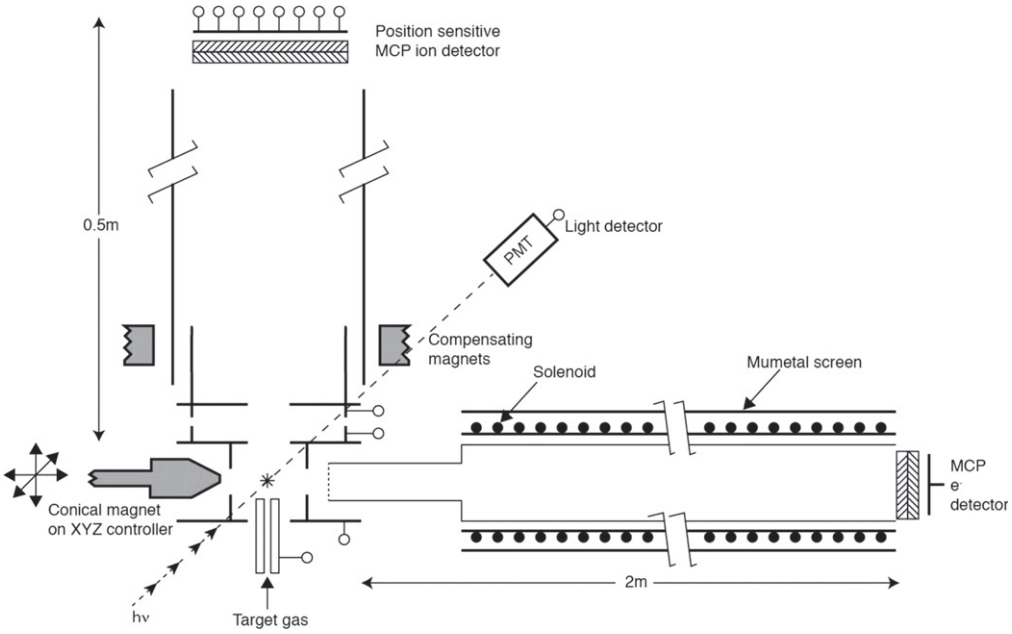

Figure 1. Schematic diagram of the apparatus, not to scale. The whole mass spectrometer section is cylindrically symmetrical about the vertical axis, centred on the gas inlet. The electrodes shown with connection points are pulsed about 20 ns after the light pulse, to allow all photoelectrons of interest to escape though the grid into the electrically field-free flight tube, before ion draw-out potentials are applied.

states. Immediately above an edge, similar resonant processes, also called satellites or shake-up states, create structures which can modify the cross-section strongly. The satellite structures in Xe are very numerous and have been examined and identified in detail by photoelectron spectroscopy [16, 17]. Because of these near-edge structures, the cross-section step method is liable to give results which depend on both the x-ray energy resolution, on the energy step size and on the exact positions at which measurements are made, as already pointed out Tawara *et al* [3]. An advantage of the present method is that the electron energy resolution for low energy electrons allows us to select pure hole states, independent of the cross-section and of the photon energy. The same method could also be used to measure the branching patterns from each satellite state separately. Because of the resolution we are able to measure branching ratios from individual spin–orbit sublevels, which has previously been done directly only in the single case of $4d^{-1}$ ionization [5]. While the electron energy resolution of the electron–ion coincidence apparatus is more than adequate for the present work, it is not quite as good as that of closely related electron-only setups [18, 19], which are therefore better suited to detailed determination of the Auger decay pathways.

Experimental

The basic scheme of the apparatus is illustrated in figure 1 which presents a new, third version of a multi-electron–ion coincidence set-up based on a magnetic bottle spectrometer (see [18, 19] and references therein). Monochromatic light from beam line U49/2 of the BESSY-II storage ring operated in single bunch mode arrives in sub-*n*s packets at a repetition rate of 1.25 MHz. To be useful for our experiments this rate is reduced to 10 kHz by a synchronous chopper [20]. The light then intersects a narrow jet of target gas within both the divergent magnetic field of a conical permanent magnet and a cylindrically symmetrical electrode array which forms a perpendicular mass spectrometer designed for velocity map imaging (VMI) [21]. In the present application, imaging was not used but mass to charge ratios were determined from the ions' time of flight. Because the strong magnetic field in the interaction region has an undesired effect on the ion trajectories, external magnets are mounted after a short distance along the ion flight path to compensate. Their effect is to centre ions of all mass-to-charge ratios effectively on the detector, though the centres for light ions, particularly H^+, are still slightly displaced. The electrons are funnelled by the field of the magnet into a long (2 m) solenoid which guides them to the distant detector, where their flight times, relative to the light pulse, are measured. Because the electric fields needed to extract ions would fatally destroy the electron energy detection, the fields are pulsed a few 10 s of ns after the light pulses, leaving time for the electrons to enter the field-free flight tube (beyond a first grid) before the pulses are applied. The arrival times of electrons and ions are recorded by multi-hit timing electronic systems, allowing any number of electrons and ions to be detected in coincidence provided they do not arrive at the same time (electrons) or at the same time and in the same position (ions). The configuration of magnetic fields constitutes a magnetic bottle [22], which ensures that almost all electrons formed at the intersection of light and target gas are guided to the detector. The total collection-detection efficiency for electrons is therefore determined largely by the detector, which comprises a *Z*-stack microchannel plate configuration. The actual efficiency is easy to determine absolutely in pure single ionization since the rates of true

electron–ion coincidences C_{ie} and the rate of ion detection E are given by:

$$C_{ie} = Nf_i f_e : \; E = Nf_i ,$$

where N is the number of ionization events, f_i is the total efficiency of ion detection and f_e is the same quantity for electrons. The quotient of these two measured rates, C_{ie}/E is equal to the electron efficiency. This scheme can be extended to multiple ionization since the rate of coincidences of an atomic ion carrying n charges with n detected electrons is $Nf_i f_e{}^n$, while the coincidence rate where only $n-1$ electrons are detected is $Nf_i f_e{}^{n-1}(1 - f_e)$. The measured ratio of these is $f_e/(1-f_e)$ from which f_e is readily derived. The total detection efficiency in these experiments was found by these methods to be 62 ± 3%, independent of energy over the range up to at least 250 eV.

Because we aim to determine the relative yields of ions in different charge states, the collection/detection efficiency for the ions is of great importance. For technical reasons, the potential of the front face of the MCP detector, which determines the energy of the ions at impact, was kept at −2350 V, which is too low to allow all Xe^{n+} ions to be detected with equal efficiency [2, 5, 23]. For some charge states the ion efficiency can be determined absolutely in the same way as for electrons, by comparing the coincidence rate with the corresponding electron rate. This works if an electron energy range can be selected where only a single ion charge state is formed in coincidence, for instance valence electrons for single ionization and isolated Auger electrons for double ionization. The relative ion efficiencies can be determined independently by comparing measured overall mass spectra at particular photon energies with reference spectra. We used the spectra of Saito and Suzuki [2] and Holland *et al* [24] for Xe and those of Tamenori *et al* [25] for Kr, which was examined as a consistency check. The relative values were used to extend our absolutely determined ion efficiencies to the more highly charged ions. The efficiencies were found to be uniformly 50 ± 5% for Xe ions with six or more charges, but less for the less highly charges ions down to only 8 ± 2% for Xe^{2+}. A check of the final values was carried out by comparison of our results with the specific branching ratios from the $4d^{-1}$ hole states of Xe (below) determined by Luhmann *et al* [5], which are in excellent agreement.

Results and discussion

Ionization from different shells

4d^{-1}. The decay of the $4d^{-1}$ hole state of Xe has been very extensively studied. The branching between single and double Auger decay was measured by Kaemerling *et al* [26] and more precisely by Luhmann *et al* [5], who determined the fraction of double Auger decay from the whole ^2D state forming Xe^{3+} as 18.8(9)%, with negligible formation of Xe^+ by optical emission. Our result for the same quantity is 17.4 ± 1%, where the error is not statistical but arises from uncertainty in the relative collection efficiencies for the low-charge ions. The two components of ^2D behave slightly differently; for double Auger decay of $^2D_{5/2}$ we find 16.3 ± 1% of Xe^{3+} (Luhmann *et al*, 16.6 ± .9%) while for $^2D_{3/2}$ our result is 20.5 ± 1% (Luhmann *et al,* 21.9 ± .9%). The calculations of Kochur *et al* [13] did not distinguish between the substates and severely underestimate the proportion of double Auger as 0.3% compared with the 16% observed. It seems that the calculations did not include all the actual pathways, including the coherent ones, revealed in electron–electron correlation maps [28]. The more recent calculations of Luhmann *et al* [5] also underestimate the same quantity as 7% or 8%. The intensities of final states formed in the single Auger decay from the $4d^{-1}$ hole states were measured by Eland *et al* [27] and those formed in double decay were identified with their branching ratios by Penent *et al* [28, 29]. Penent *et al* also showed that the double Auger decay is to a considerable extent (ca 33%) indirect, going through superexcited states of Xe^{2+} which subsequently autoionise. Such indirect processes or Auger cascades are very common if not the majority processes for most inner shells. When the photon energy is close to an inner shell edge, complex electron correlation phenomena generally called post collision interaction(PCI) occur; these have been studied in detail at the Xe 4d edge by Scheinerman *et al* [30].

4p^{-1}. The '$4p^{-1}$' appellation conceals the fact that there is no single hole state here; the underlying state is so strongly mixed with $4d^{-2}nf$ and $4d^{-2}\varepsilon f$ configurations that no sign of the $J = 1/2$ component is seen in the electron spectrum and the $J = 3/2$ peak is split into several subpeaks. The decay of this group of states has been investigated by the threshold electron–ion coincidence method [31], by Auger spectroscopy [32, 33] and by multielectron coincidence [6]. From these works it is already known that the main products are Xe^{3+} and Xe^{4+}, arising through complex Coster–Kronig Auger cascades. According to the results of threshold electron–ion coincidence [31] the formation of Xe^{4+} is 34% of the total decay of the '$4p^{-1}$ hole', while Hikosaka *et al* [6] put it at only 9% from multi-electron coincidence. Our measurements do not agree with the latter estimate, but point out that the determination is very difficult because of the nature of the electron spectra. Electron spectra, taken in coincidence with the Xe^{3+} ion at 180 and 250 eV photon energy, show a clear 4p signal as a peak with a flat, level background before and after the peak. In coincidence with Xe^{4+}, by contrast, the '4p' peak has a very strong shoulder to lower electron energy (higher binding energy) which makes it almost impossible to separate out the contribution of the peak itself. A raised background level below the peak is seen in the total electron spectra measured at both energies, and also in figure 1(a) of Hikosaka *et al* [6]. Because no Auger electrons arising from $4d^{-1}$ ionization can appear in coincidence with Xe^{4+}, only Auger electrons from 4p itself, or (at 250 eV) from $4s^{-1}$ could possibly contribute. The 4s ionization is exceedingly weak, and the only Auger decay from 4p giving Auger electrons of the necessary energy would lead to Xe^+ formation, whose measured intensity is negligible. We therefore conclude that

the interfering intensity at binding energies just above 4p arises from 4p satellites. By extracting pure peak intensities from the electron–ion coincidence spectra as best we can, we find the following decay proportions from the part of the electron spectrum most closely resembling $4p^{-1}$: Xe^{2+}; 3 ± 1.5%, Xe^{3+}; 62 ± 3%, Xe^{4+}; 35 ± 7%. This result agrees best with the ratios from threshold electron–ion coincidence [11]. The calculations of Kochur *et al* [13] agree with the experimental values to the extent that Xe^{3+} is the most abundant; the fraction of the higher charge state, Xe^{4+}, is again severely underestimated as 5.1%.

Because Hikosaka *et al* [6] and Partanen *et al* [34] have examined the electron–electron correlations connected with '$4p^{-1}$' decay in detail, we refrain from elaborating on them here. Suffice it to confirm that the Auger electrons of about 55 eV energy forming $4d^{-1}5p^{-1}$ essentially all end up as Xe^{3+}, while the group with about 32 eV all go to Xe^{4+}, as indicated in [23]. Our spectra seem at first sight to be inconsistent with Hikosaka *et al* on one other point: the threshold for formation of Xe^{4+} at both 180 and 250 eV photon energy is seen in our data as 111 ± 2 eV, which is not compatible with their value of 106.3 eV. The lower value agrees with the sum of standard ionization energies from data tables [35]. We therefore suspect that lowest level of Xe^{4+} is not formed in high abundance by the Auger cascade pathways that we observe.

4s. The cross section for populating the $4s^{-1}$ level is small, and the photoline shows in the electron spectrum at 250 eV photon energy as a weak peak on a strong background. Only when the electron spectrum is examined in coincidence with Xe^{5+} does the $4s^{-1}$ photoline stand out as the main distinct feature on a relatively smooth background. This is certainly because the ground state of Xe^{5+} lies at about 170 eV, well above 4p and all other outer shells, so apart from formation of $4s^{-1}$, the first step of any other indirect pathway to it must involve multi-electron transitions. Estimating the background contribution is again the major uncertainty in determination of the branching ratios from $4s^{-1}$; our estimates are: Xe^{3+}; 34 ± 10%, Xe^{4+}; 35 ± 8%, Xe^{5+}; 30 ± 5%. The calculations of Kochur *et al* [13] differ substantially, giving 16.5%, 77.4% and 5.1% for the same ions. The only previous experimental investigation of the decay pathways from this initial state has been the multi-electron coincidence work of Hikosaka *et al* [7], whose spectra show that it decays at least in part by a Super Coster–Kronig transition to selected $4d^{-2}$ double hole states. These states decay predominantly to Xe^{4+}, as discussed below. The ion–electron coincidence spectrum shows that while some Xe^{5+} is formed at 250 eV photon energy through $4s^{-1}$, the majority is formed by other mechanisms, as the electron peak for $4s^{-1}$ in this channel has less than 1/15 of the intensity of the background, which itself extends right down to the onset of Xe^{5+} at 170 eV. If Xe^{5+} is formed through $4s^{-1}$ there are just four more electrons to add to the spectrum and all must have energies less than about 40 eV.

3d. Decay of the $3d^{-1}$ hole states at 676 and 689 eV binding energy is seen in the high resolution M_{45}–NN Auger spectrum [9], later analysed in detail by Jonauskas *et al* [12] and in the ion yield measurements of Matsui *et al* [8] and Partanen, Sankari *et al* [11]. The Auger transitions from this hole state leave Xe species with enough energy to be ionized at least up to ninefold. The present mass spectra coincident with the individual spin–orbit levels show no measurable difference between $^2D_{5/2}$ and $^2D_{1/2}$ in branching towards the different ion states. We obtain Xe^{3+}; 4.7 ± .2%, Xe^{4+}; 53.7 ± 1%, Xe^{5+}; 25.6 ± 1%, Xe^{6+}; 13.0 ± 0.5%, Xe^{7+}; 2.4 ± .3%, Xe^{8+}; 0.4 ± .2%. These values are close to, but not in perfect agreement with those of Partanen, Sankari *et al* [11] and to those of Matsui *et al* [8]. In this case the theoretical estimates of Kochur *et al* [13] for the same ions are quite good agreement with our experimental values, at 5%, 46.0%, 31.8%, 15%, 2.1% and 0.1%. The strongest peak in the Auger electron spectra is found at about 520 eV, and is identified with the Auger transitions from $3d^{-1}$ to $4d^{-2}$, that is, creating a double hole in the 4d shell. Our electron–ion coincidence spectra show that the final states populated from the whole range of $4d^{-2}$ levels as created in this way are Xe^{4+}, 83% and Xe^{5+}, 17%. The creation and decay of the states formed with this double hole have been examined in great detail using multi-electron coincidence by Hikosaka *et al* [7], after their formation by double photoionization at 301.6 eV. This is not the main channel to Xe^{5+}, however, as our spectra show that this ion is formed mainly by population from $3d^{-1}$ via states with $4d^{-1}4p^{-1}$ and $4d^{-1}4s^{-1}$ configurations. The present coincidence data are illustrated by threefold coincidences in figure 2, which shows electron spectra coincident with both Xe^{n+} ions and photoelectrons from formation of Xe^+ $3d^{-1}(^2D_{5/2})$. The scale at the top of the figure is the binding energy of Xe^{2+} states created by the initial Auger transition from $3d^{-1}$, while the scale at the bottom is the measured electron energy. Minimum energies for appearance of the different charge states are indicated on the figure; the position of the Xe^{4+} threshold relative to the $4d^{-2}$ peak shows that both of the final two Auger electron emitted in formation of Xe^{4+} by this route are of low energy, less than 50 eV. Details of those low energy electrons are seen in the coincidence measurements of Hikosaka *et al* [7], but here they are obscured by overlap with the $3d^{-1}$ electron peaks. The major process of Xe^{5+} formation, goes via $4p^{-1}4d^{-1}$; here the three later Auger electrons share 40–80 eV between them. In the subsidiary process where Xe^{5+} is formed from $3d^{-1}$ via $4s^{-1}4p^{-1}$, one of the cascade Auger electrons has about 110 eV energy and is clearly seen as an additional peak in the spectrum (and also in complementary coincidence maps). If the 110 eV electron is the third one in this route ($3d^{-1}$ $Xe^+\{676\,eV\} \rightarrow 4s^{-1}4p^{-1}$ $Xe^{2+}\{306\,eV\} \rightarrow Xe^{3+}\{ca\ 196\,eV\} \rightarrow Xe^{5+}$, gs 162 eV) the last two electrons are again of low energy. Formation of Xe^{6+} also goes through $4s^{-1}4p^{-1}$ as the major route, and through a state of Xe^{2+} near 360 eV which could be $4s^{-2}$. In formation of the higher charge states, Xe^{7+} and Xe^{8+}, the electron spectra show little structure and even the $3d^{-1}$ lines do not stand out strongly from a continuous background, as also reported by Matsui *et al* [8].

3p. The decay of the $3p^{-1}$ states was examined by means of ion yield measurements by Saito and Suzuki [2, 36] and in the

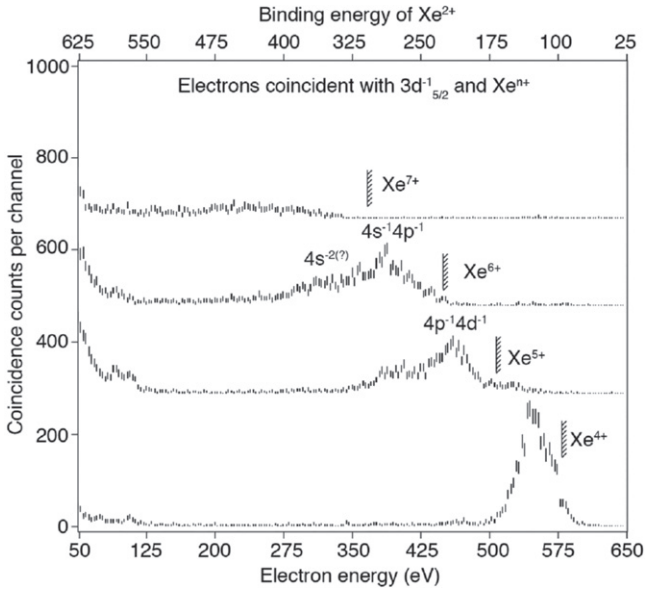

Figure 2. Spectra of electrons coincident with both an electron from $3d^{-1}(^2D_{5/2})$ ionization and the indicated Xe^{n+} ions at 710 eV photon energy. The lowest energy part is cut off because electrons from many processes pile up there, including the 3d ionizations themselves. At the high electron energies, the energy scale should be read as indicative rather than exact, because the calibration is less reliable in this region. The strong peak coincident with Xe^{4+} comes from intermediate formation of $Xe^{2+}(4d^{-2})$ as discussed in the text. Intermediate ionizations involved in formation of the other ions are indicated.

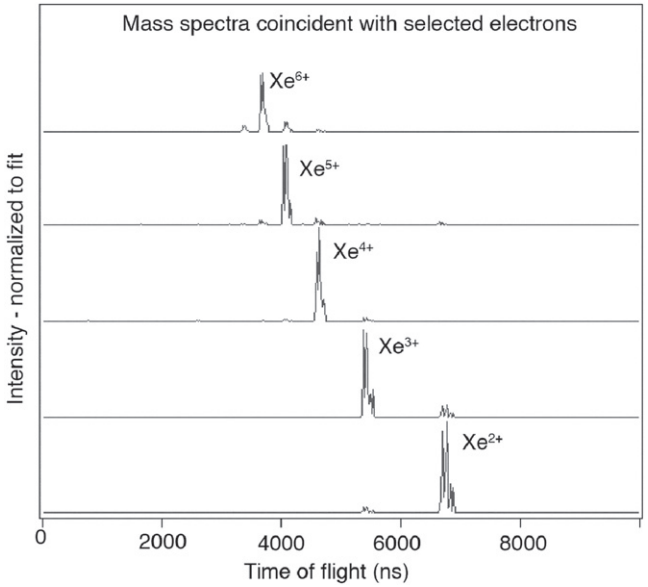

Figure 3. Mass spectra coincident with selected numbers and energies of electrons. For Xe^{2+}, Auger electrons of around 33 eV are selected at 110 eV photon energy. For Xe^{3+} three electrons with summed energy between the estimated appearance energy of the ion and the ion of next higher charge are chosen. For Xe^{4+} we take electrons in the main Auger peak at 550 eV in coincidence with $3d_{5/2}^{-1}$, at 710 eV. For Xe^{5+} at 710 eV, four electrons with energy sum between 475 and 535 eV are taken and finally for Xe^{6+} we select one electron between 300 and 350 eV together with the $3d_{5/2}^{-1}$ photoline.

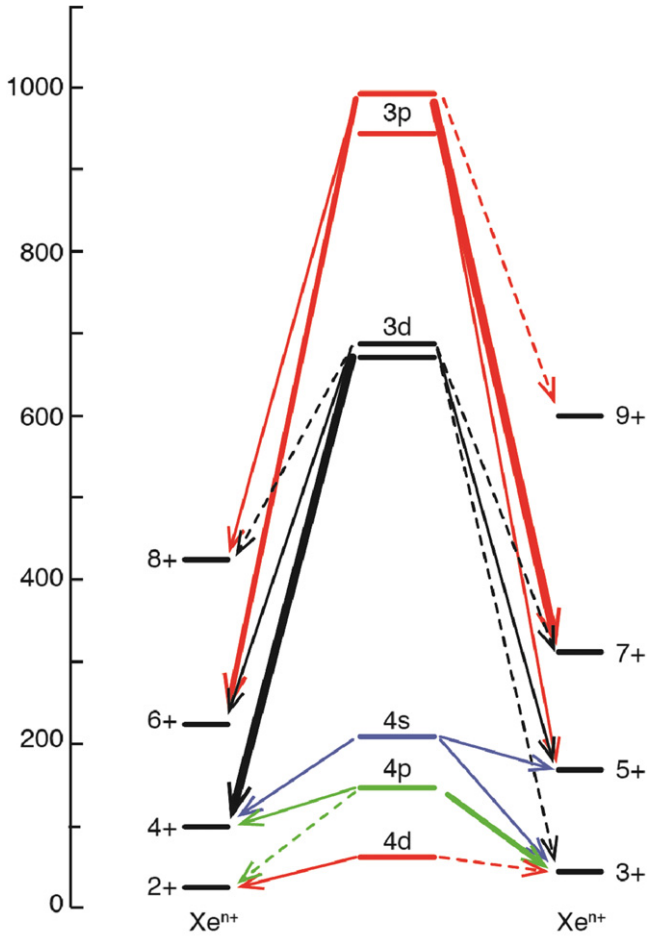

Figure 4. Graphical representation of the branching to different charge states of Xe from individual shells as lines of different thickness with very low intensity as dashed lines. Subshells are not distinguished and only the minimum energy for production of each charge is shown. For charge states higher than 5+ the energies marked are theoretical estimates [38] as exact experimental values are not available.

early estimates by Carlson *et al* [37]. The $^2P_{3/2}$ and $^2P_{1/2}$ levels at 941 and 1002 eV are clearly visible at 1200 eV photon energy, but with a non-statistical relative intensity ratio of 5:1. The decay patterns from the two levels are detectably different:

	4+	5+	6+
$^2P_{3/2}$	3 ± .8	16.8 ± .8	28.3 ± 2
$^2P_{1/2}$	3.2 ± 1.5	9.1 ± 2.2	27.2 ± 3.3
	7+	8+	9+
	38.6 ± 2	11.5 ± 1.5	1.7 ± .6%
	39.6 ± 3.6	16.4 ± 2.4	4.5 ± 1%.

The overall pattern predicted by the theoretical calculations of Kochur *et al* [13] is in fair agreement with these figures, as is the prediction of a difference between $^2P_{3/2}$ and $^2P_{1/2}$, but there are differences of detail and the abundance of the highest charge states is underestimated. The higher yields

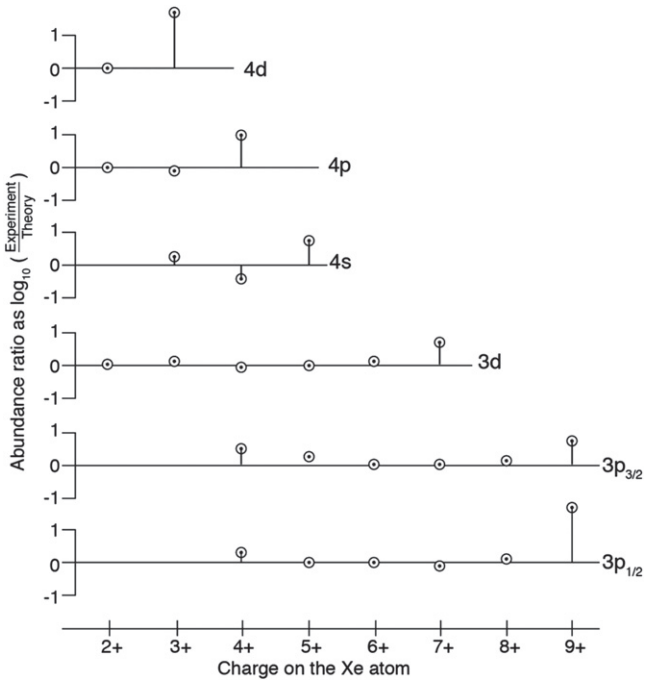

Figure 5. Comparison of the branching fractions predicted by the Hartree–Fock calculations of Kochur *et al* [13] with our measured branching fractions. The vertical scales show the common logarithm of the experimental fraction divided by the calculated one.

of Xe^{8+} and Xe^{9+} from $^2P_{1/2}$ seem unlikely to be explicable simply from their energies relative to the thresholds for forming the two ions, which must be near 430 and 606 eV respectively [35] and thus well below the $3p^{-1}$ levels. Unfortunately our electron spectra at the energies where $3p^{-1}$ levels are formed do not have good enough statistics to allow us to deduce detailed decay pathways. The Coster–Kronig transition $3p^{-1} \rightarrow 3d^{-2}$, which would otherwise be favoured, is energetically forbidden. There is a clear peak at about 180 eV in the electron spectrum coincident with ions and the $^2P_{3/2}$ photoline, suggesting that the transition $3p_{3/2}^{-1} \rightarrow 3d^{-1}4d^{-1}$ plays a role as a first step in the cascades leading to the more highly charged ions. (We estimate the energy of the $3d^{-1}4d^{-1}$ states by adding the individual orbital binding energies to an estimated Coulomb repulsion term as $680 + 68 + 10 = 758$ eV so the expected Auger energy is $941 - 758 = 183$ eV.)

Selection of individual charge states

By selection based on the presence of coincident electrons in the right numbers and of the appropriate energies, it should ideally be possible to choose any individual degree of ionization. In practice this is easy for relatively low charge states, but more difficult for higher ones. Part of the difficulty is purely technical and hopefully temporary; our present electronics do not register electrons separately when they arrive close together in time, so some electrons are missed, particularly at high energies where arrival times bunch together. Furthermore, even with high collection efficiency f_e for individual electrons, the overall efficiency for n electrons, f_e^n becomes very small when n is high. For the higher charges we cannot therefore isolate n-fold ionization by requiring detection of n electrons of the correct energy sum. Instead we try to choose particular electrons which identify cascades leading to the desired final state. The present degree of success is illustrated in figure 3 where the less perfect selection of the higher charges is evident.

Conclusions

In this work we have commissioned new apparatus capable of detecting multiple electrons and ions in coincidence, with good resolution for both ion mass and electron energy. By using it we have measured the branching patterns to final charge states of Xe from pure inner-shell hole states from the 4d to the 3p shells, with resolution of the spin–orbit substates. The branching is illustrated graphically in figure 4 in relation to the minimum energy for production of each final charge on the Xe atom, showing that the highest energetically accessible charge is reached from the shallower inner shell holes, but not from 3d or 3p. We believe that these are the most comprehensive and reliable data available on these quantities, and provide both a challenge to theory and a guide for future experiments. Comparison of the branching fractions with those predicted by rather comprehensive Hartee–Fock calculations [13] is made graphically in figure 5, which shows that the calculations make accurate predictions for all but the highest charges. The proportion of the highest charge states is severely underestimated in every single case. Higher level calculations are scarce, but those we are aware of still underestimate the formation of the most highly charged ions,

Table 1. Percentage branching to Xe^{n+} ion states after hole creation in inner shells.

	$4d_{5/2}$	$4d_{3/2}$	'4p'	4s	3d	$3p_{3/2}$	$3p_{1/2}$
Xe^{2+}	83.7 ± 1	79.5 ± 1	3 ± 1.5				
Xe^{3+}	16.3 ± 1	20.5 ± 1	62 ± 3	34 ± 10	4.7 ± .2		
Xe^{4+}			35 ± 7	35 ± 8	53.7 ± 1	3 ± .8	3.2 ± 1.5
Xe^{5+}				30 ± 5	25.6 ± 1	16.8 ± .8	9.1 ± 2.2
Xe^{6+}					13 ± .5	28.3 ± 2	27.2 ± 3.3
Xe^{7+}					2.4 ± .3	38.6 ± 3.6	39.6 ± 3.6
Xe^{8+}					0.4 ± .2	11.5 ± 1.5	16.4 ± 2.4
Xe^{9+}						1.7 ± .6	4.5 ± 1

though less severely. It seems likely that to accurately represent the multi-electron as well as multi-step processes involved, inclusion of electron correlation must be necessary in addition to some relativistic corrections. None of the extant calculations include coherent 2-electron double Auger processes, which are certainly significant in addition to stepwise pathways, particularly for the 4d shell, as demonstrated by electron–electron correlations [28]. For the deeper inner shell holes, where Coster–Kronig transitions are dominant, coherent two-electron decay is less significant, but still contributes particularly to formation of the most highly charged ions.

The branching patterns to final charges states of Xe, as measured in this work and collected in table 1, are a prototype for creation of highly charged molecules by inner shell ionization of substituent heavy atoms such as iodine. In molecules, an additional step, possible at all stages of the Auger cascades, will be intramolecular charge transfer. Timing experiments with femtosecond resolution will be needed to characterise the charge evolution in detail and its likely competition with nuclear motion. By selecting the ejected electrons by number and energy, we have shown that predominantly single charge states can potentially be selected; the ability to do this for molecular ionization will be a great asset in a forthcoming systematic study of the dynamics of Coulomb explosions.

Acknowledgments

This work has been financially supported by the Swedish Research Council (VR) and the Knut and Alice Wallenberg Foundation, Sweden. We acknowledge the technical assistance of John Freeman in preparing this publication. We thank the Helmholtz Zentrum Berlin for the allocation of synchrotron radiation beam time and the staff of BESSY II for particularly smooth running of the storage ring in top-up mode during the single-bunch runtime. The research leading to these results has received funding from the European Community's Seventh Framework Programme (FP7/2007-2013) under grant agreement no. 312284.

References

[1] Becker U *et al* 1989 *Phys. Rev.* A **39** 3902
[2] Saito N and Suzuki I H 1992 *Int. J. Mass Spectrom. Ion Process.* **115** 157
[3] Tawara H *et al* 1992 *J. Phys. B: At. Mol. Opt. Phys.* **25** 1467
[4] Tonuma T *et al* 1987 *J. Phys. B: At. Mol. Phys.* **20** L31
[5] Luhmann T *et al* 1998 *Phys. Rev.* A **57** 282
[6] Hikosaka Y *et al* 2007 *Phys. Rev.* A **76** 032708
[7] Hikosaka Y *et al* 2007 *Phys. Rev. Lett.* **98** 183002
[8] Matsui T *et al* 2004 *J. Phys. B: At. Mol. Opt. Phys.* **37** 3745
[9] Werme L O, Bergmark T and Siegbahn K 1972 *Phys. Scr.* **6** 141
[10] Partanen L *et al* 2006 *J. Phys. B: At. Mol. Opt. Phys.* **39** 4515
[11] Partanen L *et al* 2005 *J. Phys. B: At. Mol. Opt. Phys.* **38** 1881
[12] Jonauskas V *et al* 2003 *J. Phys. B: At. Mol. Opt. Phys.* **36** 4403
[13] Kochur A G *et al* 1994 *J. Phys. B: At. Mol. Opt. Phys.* **27** 1709
[14] Eland J H D and Feifel R 2006 *Chem. Phys.* **327** 85
[15] Samson J A R and Haddad G N 1974 *Phys. Rev. Lett.* **33** 875
[16] Kikas A *et al* 1996 *J. Electron Spectrosc. Relat. Phenom.* **77** 241
[17] Alitalo S *et al* 2001 *J. Electron Spectrosc. Relat. Phenom.* **114-116** 141
[18] Feifel R, Eland J H D, Storchi L and Tarantelli F 2006 *J. Chem. Phys.* **125** 194318
[19] Eland J H D, Linusson P, Mucke M and Feifel R 2012 *Chem. Phys. Lett.* **548** 90
[20] Plogmaker S *et al* 2012 *Rev. Sci. Instrum.* **83** 03115
[21] Eppink A T J B and Parker D H 1997 *Rev. Sci. Instrum.* **68** 3477
[22] Kruit P and Read F H 1983 *J. Phys. E: Sci. Instrum.* **16** 313
[23] Hayaishi T *et al* 1984 *J. Phys. B: At. Mol. Phys.* **17** 3511
[24] Holland D M P *et al* 1979 *J. Phys. B: At. Mol. Phys.* **12** 2465
[25] Tamenori Y *et al* 2004 *J. Phys. B: At. Mol. Opt. Phys.* **37** 117
[26] Kaemmerling B *et al* 1992 *J. Phys. B: At. Mol. Opt. Phys.* **25** 3621
[27] Eland J H D *et al* 2003 *Phys. Rev. Lett.* **90** 053003
[28] Penent F *et al* 2005 *Phys. Rev. Lett.* **95** 083002
[29] Penent F *et al* 2005 *J. Electron Spectrosc. Relat. Phenom.* **144** 7
[30] Scheinerman S *et al* 2006 *J. Phys. B: At. Mol. Opt. Phys.* **39** 1017
[31] Hayaishi T *et al* 2002 *J. Phys. B: At. Mol. Opt. Phys.* **35** 141
[32] Heinaesmaeki S *et al* 2004 *J. Electron Spectrosc. Relat. Phenom.* **137–140** 281
[33] Kivimaeki A *et al* 1998 *J. Electron Spectrosc. Relat. Phenom.* **93** 89
[34] Partanen L *et al* 2007 *J. Phys. B: At. Mol. Opt. Phys.* **40** 4605
[35] Kramida A *et al* 2014 NIST *Atomic Spectra Database* version 5.2
[36] Saito N and Suzuki I H 1992 *J. Phys. B: At. Mol. Opt. Phys.* **25** 1785
[37] Carlson T A, Hunt W E and Krause M O 1966 *Phys. Rev.* **151** 41
[38] Borovik A 2010 *Doctoral Thesis* Justus-Liebig University, Giessen